

# Seasonal-varying characteristics of tropical Pacific westerly wind bursts during El Niño due to annual cycle modulation

Zhuolin Xuan<sup>1,2</sup> · Wenjun Zhang<sup>1</sup> · Feng Jiang<sup>1</sup> · Malte F. Stuecker<sup>3</sup> · Fei-Fei Jin<sup>4</sup>

Received: 6 April 2023 / Accepted: 25 July 2023 / Published online: 14 August 2023 © The Author(s), under exclusive licence to Springer-Verlag GmbH Germany, part of Springer Nature 2023

#### **Abstract**

Westerly wind bursts (WWBs), aperiodic burst-like atmospheric disturbances in the tropics, play an important role during the development stage of El Niño–Southern Oscillation (ENSO) events and in turn can be strongly modulated by ENSO itself. Previous work argued that WWBs exhibit a pronounced seasonality at the equator during an El Niño evolution, i.e., being more frequent and vigorous during the developing boreal autumn compared to the decaying spring. Here we show that this seasonal difference in WWB activity at the equator is a segmentary manifestation of a meridional migration of WWB activity, which is closely linked to the southward displacement of the El Niño-related deep convection from the developing autumn to decaying spring. The highest climatological SSTs over the western-central Pacific are located mainly to the north of the equator in boreal autumn and south of it during boreal spring; hence the equatorially quasi-symmetric El Niño-related SST anomalies tend to induce deep convection and generate more WWBs in the Northern Hemisphere during the developing autumn and more in the Southern Hemisphere during the decaying spring. Despite some differences in the zonal distribution and intensity, there appears a close resemblance between the seasonal-varying features of WWBs during eastern Pacific (EP) and central Pacific (CP) El Niño events regarding the north–south displacement, due to similar meridional shifts of deep convection anomalies. This study provides a more comprehensive picture of the spatiotemporal characteristics of WWBs during El Niño events and improves our understanding of the relationship between ENSO and high-frequency atmospheric variability.

Keywords Westerly wind burst · El Niño · Meridional migration · Annual-cycle modulation

- Wenjun Zhang zhangwj@nuist.edu.cn
- CIC-FEMD/ILCEC, Key Laboratory of Meteorological Disaster of Ministry of Education, School of Atmospheric Sciences, Nanjing University of Information Science and Technology, Nanjing 210044, China
- Zhejiang Meteorological Observatory, HangZhou 310017, China
- Department of Oceanography and International Pacific Research Center (IPRC), School of Ocean and Earth Science and Technology (SOEST), University of Hawai'I at Mānoa, Honolulu, HI, USA
- Department of Meteorology, School of Ocean and Earth Science and Technology, University of Hawai'I at Mānoa, Honolulu, HI, USA

### 1 Introduction

Westerly Wind Bursts (WWBs) refer to high-frequency westerly wind anomalies across the tropical oceans, usually concurrent with a large cluster of deep convection (e.g., Hartten 1996; Harrison and Vecchi 1997; Seiki and Takayabu 2007; Fu and Tziperman 2019, 2021). Previous studies have shown that WWBs, in particular those occurring over the equatorial western and central Pacific, exert pronounced impacts on the commencement of El Niño events (e.g., McPhaden 1999; Boulanger et al. 2001; Lengaigne et al. 2004; Fedorov et al. 2015; McGregor et al. 2016; Lian and Chen 2021). WWBs can excite downwelling oceanic Kelvin waves that propagate eastward and generate warm sea surface temperature (SST) anomalies in the eastern equatorial Pacific via the thermocline feedback, which can develop further into an El Niño event. Beyond this, WWBs can also drive anomalous surface zonal currents, transporting warm water from the western to central Pacific



and thereby contribute to the El Niño development via the advective feedback. So far, it has been well recognized that WWBs can modulate ENSO in terms of its irregularity, asymmetry, and intensity (e.g., Fedorov et al. 2015; Chen et al. 2015; Levine et al. 2016; Hayashi and Watanabe 2017, 2019; Lian and Chen 2021; Yu and Fedorov 2020).

Instead of treating WWBs as a stochastic atmospheric process independent of the background ocean condition (Battisti and Sarachik 1995; Kleeman and Moore 1997), many previous studies identified a deterministic element in WWBs that is modulated by the underlying large-scale SST patterns (Harrison and Vecchi 1997; Eisenman et al. 2005; Gebbie et al. 2007; Seiki and Takayabu 2007; Puy et al. 2016). WWBs are prone to occur over the western Pacific warm pool region with high background SSTs that favor the excitation of the deep convection. Due to the meridional march of solar insolation, WWBs experience a strong seasonality along with seasonal-varying climatological SSTs, featuring frequent occurrence in the Northern Hemisphere during boreal summer and autumn and in the Southern Hemisphere during boreal winter and spring (Harrison and Giese 1991; Harrison and Vecchi 1997). Many observational analyses have also shown that the temporal and spatial features of WWBs are closely related to the ENSO-associated SST anomalies in the tropical Pacific on interannual timescales (Eisenman et al. 2005; Seiki and Takayabu 2007). During El Niño years, the associated warm SST anomalies can stretch the warm pool's eastern edge into the central-to-eastern Pacific. Correspondingly, WWBs extend further eastward and occur more frequently and vigorously (Eisenman et al. 2005; Gebbie et al. 2007; Tziperman and Yu 2007; Chen et al. 2015). El Niño is also known to exhibit a remarkable seasonal synchronization with the annual cycle, which usually starts evolving in boreal spring, develops during summer and autumn, reaches its peak in winter, and then decays rapidly in the following spring (Rasmusson and Carpenter 1982; Stein et al. 2010, 2014). During different phases of El Niño, the activity of WWBs appears to be distinctively different in terms of both frequency and strength. Some previous studies showed that more frequent and vigorous WWBs occur at the equator during the developing autumn than the decaying spring of El Niño despite comparable magnitude of SST anomalies (e.g., Seiki and Takayabu 2007; Sun et al. 2020). This seasonal difference in the high-frequency variability over the equatorial Pacific was argued to be associated with the asymmetric strength of the equatorial Rossby and mixed Rossby gravity waves (Sun et al. 2020). Considering the observed fact that the climatological features of WWBs exhibit a remarkable meridional migration along with the march of solar insolation, this seasonality of WWBs at the equator needs to be revisited by expanding our focus into a wide latitudinal band to obtain a more comprehensive picture of the spatiotemporal characteristics of WWBs during El Niño events.

Besides, the central Pacific (CP) El Niño event has been observed more frequently in recent decades, which is dramatically different from traditional El Niño events during which the SST anomaly center is typically confined to the eastern Pacific (EP) (e.g., Fu et al. 1986; Larkin and Harrison 2005; Ashok et al. 2007; Kao and Yu 2009; Kug et al. 2009; Ren and Jin 2011). These two flavors of El Niño exhibit contrasting interactions with the western Pacific SST annual cycle, which leads to different meridional shifts of the associated atmospheric response from developing autumn to decaying spring (e.g., McGregor et al. 2012, 2013; Stuecker et al. 2013, 2015; Zhang et al. 2015; Jiang et al. 2020). Specifically, the southward shift and the associated weakening of zonal wind anomalies at the equator are typically more prominent during EP El Niño events than CP El Niño events (e.g., Zhang et al. 2015; Jiang et al. 2020; Gong and Li 2022). Hence, it is compelling to ask whether the spatiotemporal characteristics of the high frequency part of wind anomalies such as WWBs show similar differences for the two different flavors of El Niño.

In the present work, we investigate the seasonal-varying features of WWBs over the tropical Pacific during El Niño and potential differences during the two different El Niño flavors. We find that the activity of WWBs during El Niño is shifted southward along with the seasonally modulated El Niño-related deep convection, due to the interaction of El Niño and background high SSTs. Moreover, WWB activity features similar meridional displacements during the two different flavors of El Niño events, being controlled by the same dynamical process. The remainder of this paper is structured as follows. Section 2 introduces the data and methodology utilized in this study. Section 3 displays the spatiotemporal characteristics of WWBs during El Niño events, especially their meridional shift and the associated variations at the equator. The possible mechanisms are explored in Sect. 4. The seasonal-varying features of WWBs for different El Niño types are then investigated and compared in Sect. 5. Finally, Sect. 6 provides the main conclusion and discussion.

### 2 Data and methodology

To investigate the spatiotemporal features of WWBs, we utilize daily averaged wind at 10-m altitude from the European Centre for Medium-Range Weather Forecasts (ECMWF) Reanalysis Version 5 dataset (ERA5; Hersbach et al. 2020). Daily outgoing longwave flux (OLR) data are also obtained from ERA5 reanalysis (Hersbach et al. 2020). The daily SST data is from the NOAA high-resolution



blended analysis of Optimum Interpolation SST version 2 (OISST v2; Reynolds et al. 2007). The spatial resolution is  $0.5^{\circ} \times 0.5^{\circ}$  for all datasets. All anomalies are calculated by removing the climatology over the entire period (1982–2020) and are linearly detrended to exclude possible influences from global warming. To avoid the possible impacts of the decadal signal, we also apply a 10-year highpass filter to all datasets and find that our main conclusion remains almost the same (not shown). Statistical significance is inferred based on a two-tailed Student's test.

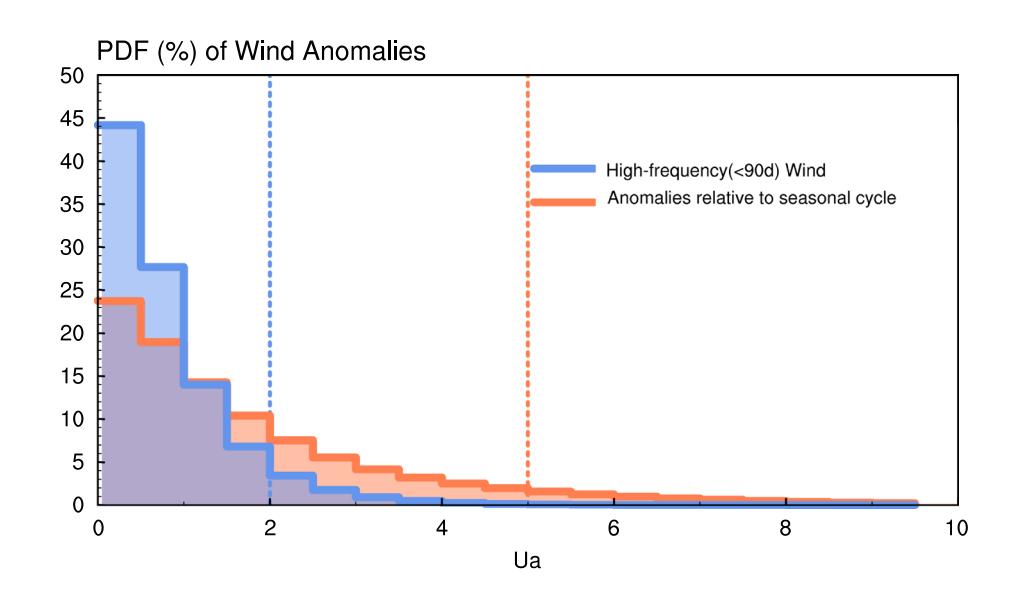
The El Niño events are identified when the 3-month running mean Niño3.4 index (averaged SST anomaly in the region of 5°S-5°N, 120°-170°W) is larger than 0.5 °C for five consecutive months, consistent with the Climate Prediction Center's definition. Twelve El Niño events (1982/83, 1986/87, 1991/92, 1994/95, 1997/98, 2002/03, 2004/05, 2006/07, 2009/10, 2014/15, 2015/16, 2018/19) are identified during 1982-2020. The El Niño events are represented as year (0)/year (1), where numerals "0" and "1" denote the developing and decaying year, respectively. We further categorized these events into two flavors—three EP El Niño events (1982/83, 1997/98, 2015/16) and nine CP El Niño events (1986/87, 1991/92, 1994/95, 2002/03, 2004/05, 2006/07, 2009/10, 2014/15, 2018/19), based on the cold tongue and warm pool indices ( $N_{CT}$  and  $N_{WP}$ ) in boreal winter (November–December–January; NDJ) (Ren and Jin 2011). These indices are devised through a simple transformation of Niño3 (N3; SST anomaly in the region of 5°S-5°N, 90°-150°W) and Niño4 (N4; SST anomaly in the region of 5°S-5°N, 160°E-150°W) indices as shown in Eq. (1):

$$\begin{cases} N_{CT} = N3 - \alpha N4 \\ N_{WP} = N4 - \alpha N3 \end{cases} \alpha = \begin{cases} 0.4 = N3N4 > 0 \\ 0 \quad otherwise \end{cases}$$
 (1)

Fig. 1 The probability histogram (%) of zonal wind anomalies relative to the seasonal cycle (orange) and 90-days high-pass filtered wind anomalies (blue) in the region of 5°S-5°N, 120°E-80°W. Here, the wind anomalies are binned to every 0.5 m/s, and then the corresponding probabilities are calculated. The dashed lines indicate the magnitude criteria of the upper 7.5%

The El Niño events are defined as EP El Niño if  $N_{CT}$  is greater than  $N_{WP}$  and CP El Niño if  $N_{CT}$  is less than  $N_{WP}$ .

In this study, WWBs over the tropical Pacific are identified by using the daily zonal wind at 10-m altitude following previous studies (Harrison and Vecchi 1997; Seiki and Takayabu 2007; Chiodi et al. 2014). With particular emphasis on the meridional migration of WWBs, we regridded the raw wind onto the grid of 1 degree in latitude and 10 degrees in longitude by using the bilinear interpolation method. Previously, WWBs were commonly defined by analyzing the wind anomalies with respect to the mean seasonal cycle (e.g., Harrison and Vecchi 1997; Seiki and Takayabu 2007). Recently, to avoid confusion with low-frequency wind anomalies, WWBs have often been identified based on the high-pass filtered data with a cutoff of less than about 90 days (Puy et al. 2016; Capotondi et al. 2018). Considering the potential sensitivity of the ENSO-WWB relationship to different WWB definitions (e.g., Capotondi et al. 2018; Lian et al. 2021), the above two detection methods are both used in this study to ensure the robustness of our results. In the first method (M1), WWBs at each grid point are identified when wind anomalies relative to the seasonal cycle are stronger than 5 m/s with the duration of three days at least. This threshold corresponds to the upper 7.5% of magnitude of westerly wind anomalies over the tropical Pacific (5°S-5°N,120°E-80°W) as shown in Fig. 1. The same proportion is consistently used to define the threshold (i.e., 2 m/s) of the WWBs in the high-frequency zonal wind anomalies. Hence, WWBs are defined as the 90-day highpass filtered wind with the intensity higher than 2 m/s and a duration longer than 3 days in the second method (M2). Qualitative conclusion remains the same if the zonal and meridional resolutions vary slightly. Two measurements are used to characterize the features of WWBs, one of which is the WWB frequency (days with WWBs per month), and





the other of which is the accumulated WWB strength (time integration of zonal wind anomalies associated with WWBs; m/s per month). These measurements synthetically consider the characteristics of WWBs in aspects of the zonal extension, duration, and amplitude of the zonal wind anomalies (e.g., Hartten 1996; Seiki and Takayabu 2007; Gebbie et al. 2007; Liang et al. 2021).

## 3 Spatial-temporal characteristics of WWBs during El Niño

We firstly show the composite evolution of the SST anomaly and WWB frequency at the equator in M1 during El Niño events (Fig. 2a). The El Niño event generally starts evolving in boreal spring and tends to reach its peak during boreal winter with positive SST anomalies centered around 120°W. With respect to the El Niño peak phase, the composite SST anomalies display relatively symmetric features during the developing and decaying

phases from August(0) to April(1). Despite the comparable magnitude of SST anomalies, the occurrence of equatorial WWBs shows an obvious seasonal difference between the developing autumn (August–September–October; ASO(0)) and decaying spring (February–March–April; FMA(1)) seasons. During ASO(0), the frequency of WWBs over the entire equatorial Pacific is increased by ~ 150% compared to the climatology. In comparison, the WWB frequency during FMA(1) is much weaker, which is increased by nearly 50% relative to the climatology (Fig. 2b). A similar seasonality of WWBs at the equator is also shown in the accumulated strength (Fig. 2c-d), consistent with previous studies (Seiki and Takayabu 2007; Sun et al. 2020). We further investigate the frequency and accumulated strength of WWBs at the equator defined by M2 to test the robustness of this seasonal decrease of equatorial WWBs (Fig. 2e-h). The same seasonality of WWBs can be derived during El Niño events, suggesting this seasonal characteristic is not dependent on the specific definitions.

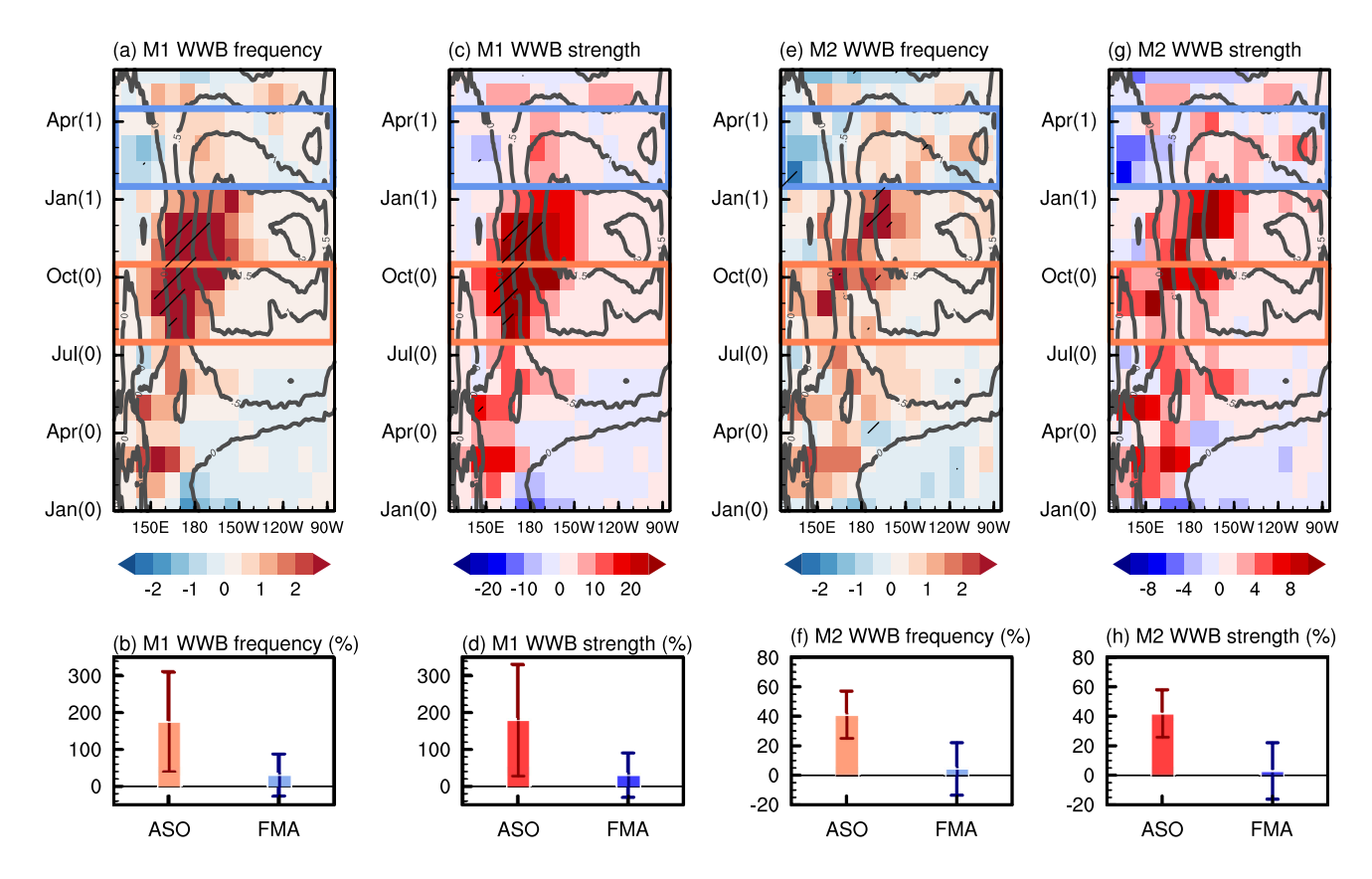


**Fig. 2** a Composite time-longitude evolution of the equatorial averaged (0.5°S-0.5°N) SST anomaly (°C; contours at intervals of 0.5 °C) and the WWB frequency anomaly (days per month; shading) based on M1 during the El Niño events. **c** Same as **a** except for the accumulated strength anomaly (m/s per month; shading). Hatching indicates composite values that exceed the 90% significance level. The orange and blue boxes represent the El Niño developing autumn (ASO(0))

and decaying spring (FMA(1)), respectively. The percentage of the anomalous WWB frequency  $\mathbf{b}$  and accumulated strength  $\mathbf{d}$  relative to the climatology over the equatorial Pacific (120°E-80°W) during the El Niño ASO(0) and FMA(1) in M1. The orange and blue error bars denote one standard deviation error estimates for ASO(0) and FMA(1), respectively.  $\mathbf{e}$ - $\mathbf{h}$  As in  $\mathbf{a}$ - $\mathbf{d}$ , but for WWBs defined by high-frequency wind anomalies (M2)



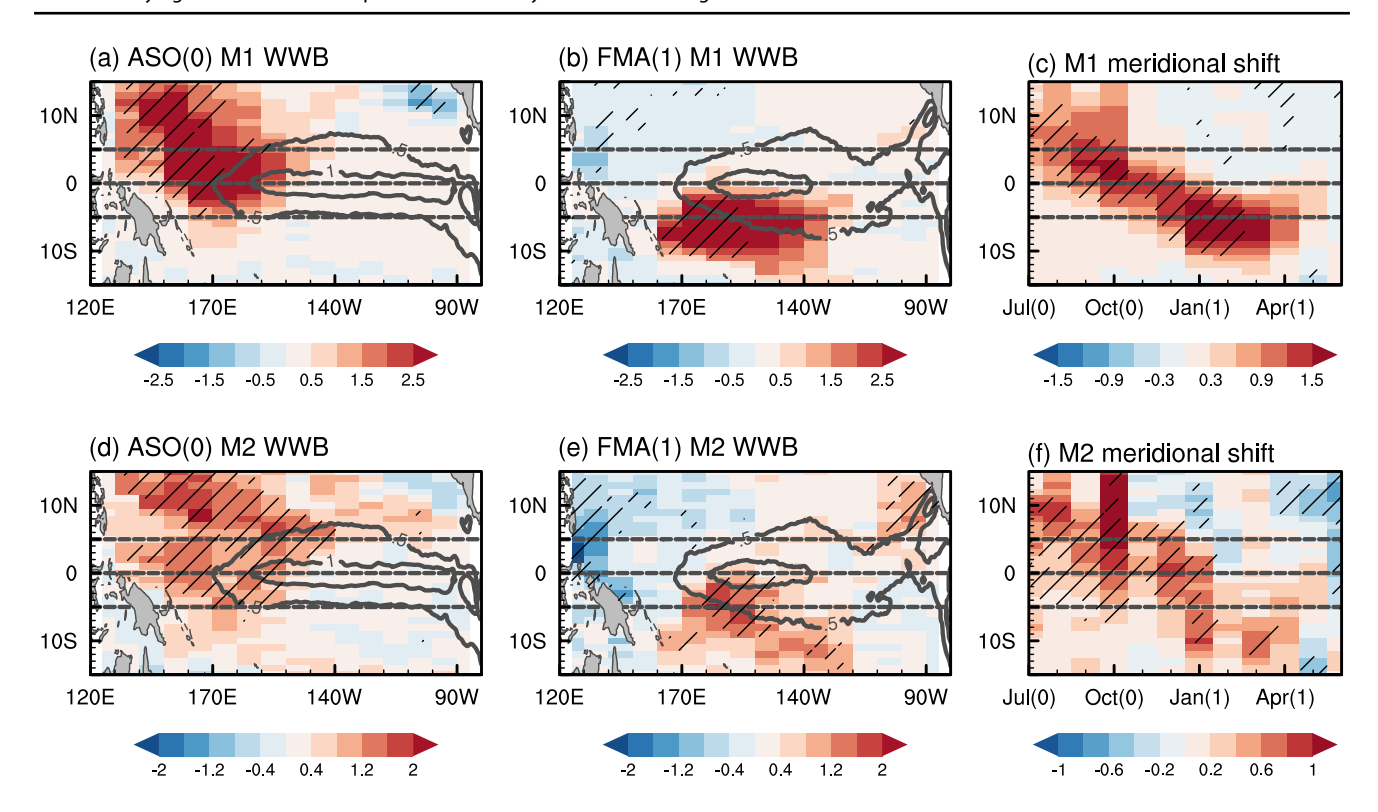


**Fig. 3** Composite spatial distribution of the frequency anomaly of WWB defined by M1 (days per month; shading) and SST anomaly (°C; contours at intervals of 0.5 °C with zero contours omitted) during **a** ASO(0) and **b** FMA(1) of El Niño. **c** Latitude–time section

of the WWB frequency anomaly averaged over the tropical Pacific (120°E-80°W) for El Niño events. **d**–**f** As in **a**–**c**, but for the WWB defined by M2. Hatching indicates composite values that exceed the 90% significance level

To inspect the full spatiotemporal characteristics of WWBs, we in Fig. 3 display the spatial patterns of the frequency and accumulated strength of WWBs defined by M1 and M2 during El Niño developing and decaying phases. Here the accumulated strength of WWBs is not shown considering their similar distribution to the WWB frequency. During ASO(0), WWBs are frequently observed over the Western North Pacific (WNP) and the equatorial western Pacific with the maximum of WWB frequency being more than 0.5 per month around 3°N, 160°E (Fig. 3a). When the El Niño events enter their decaying spring (Fig. 3b), the WWB activity is displaced southward with the center located at about 5°S. The seasonal-varying behaviors of WWBs are also seen in the spatial distribution of WWB frequency defined by M2 (Fig. 3d-e). We further show the zonally averaged (120°E-80°W) latitude-time distribution of WWB frequency in M1 and M2, and both of them clearly exhibit southward migration across the equator (Fig. 3c, f). It is mentioning that the seasonal-varying feature of anomalous WWB activity aligns with that of climatological WWBs (Harrison and Giese 1991; Harrison and Vecchi 1997), with a strong phase-locking characteristic to the annual cycle. The seasonal-varying features of WWBs are consistent with previous studies on the abrupt southward

shift of wind and related weakening of wind anomalies at the equator (e.g., Harrison 1987; Harrison and Larkin 1998; McGregor et al. 2012), which is a manifestation of the ENSO Combination Mode (Stuecker et al. 2013). In this context, the previously mentioned seasonal difference of WWBs at the equator is a segmentary manifestation of the meridional migration over the tropical Pacific, which could lead to the one-sided view that a distinct seasonal difference of the WWB activity exists when focusing on the equator.

### 4 Possible mechanism for the meridional shifts of WWBs

So far, our observational analysis showed that the anomalous activity of WWBs experiences a strong southward shift from the developing autumn to decaying spring of El Niño. We next investigate the possible mechanism responsible for this meridional shift of the WWB activity along with the El Niño evolution and find that this southward migration is associated with a shift in deep convection. Previous studies have shown that atmospheric deep convection anomalies, associated with tropical cyclones, the Madden–Julian Oscillation, and extratropical cold surges (e.g., Chu 1988; Keen 1982; Nitta 1989;



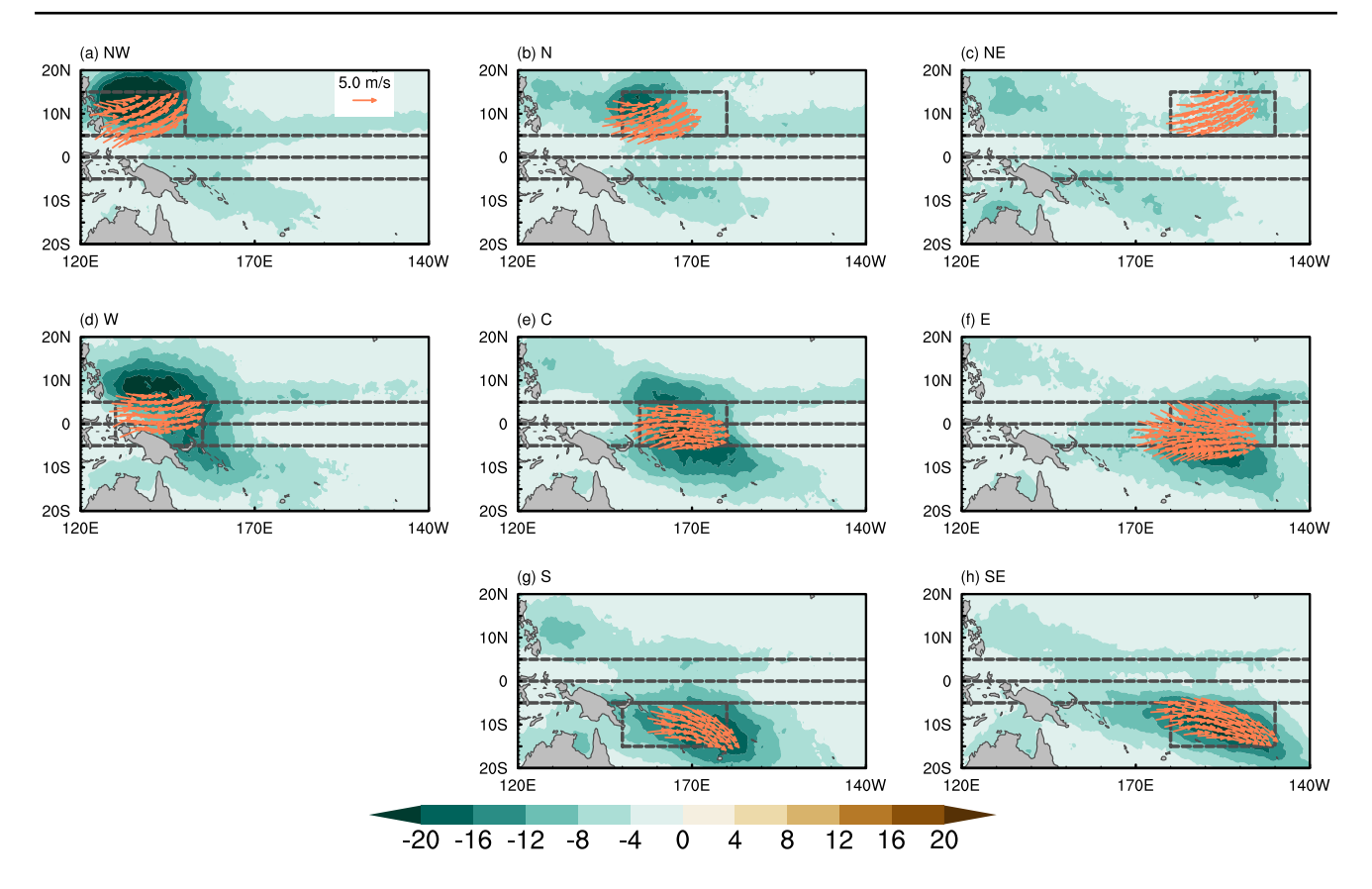


Fig. 4 Composite outgoing longwave radiation anomalies (W/ $m^2$ ; shading) which satisfy the criterion for deep convections (OLR < 170W/ $m^2$ ) and zonal wind anomalies (m/s; vector) during days when WWBs occur at any grid point over the **a** northwestern,

**b** northern, **c** northeastern, **d** western, **e** central, **f** eastern, **g** southern, and **h** southeastern region of the tropical Pacific. Wind anomalies that are less than 4 m/s are not shown

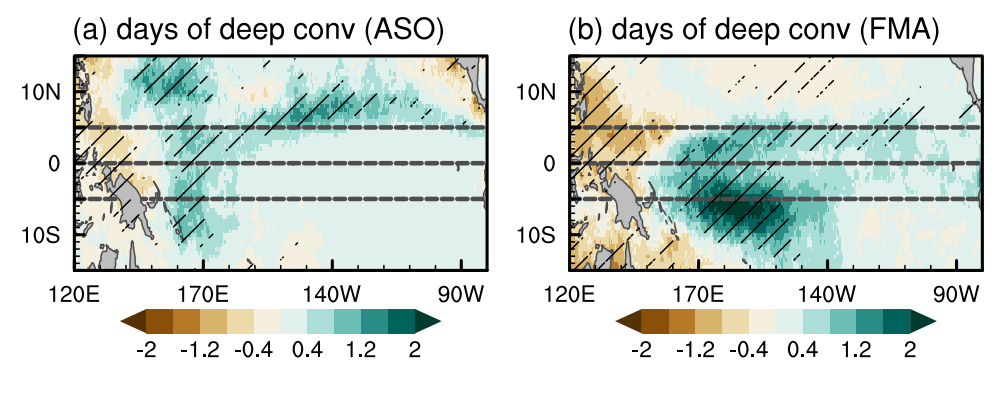
Lian et al. 2018), usually play a major role in generating WWBs (e.g., Meehl et al. 1996; Hartten 1996; Fasullo and Webster 2000). To demonstrate the possible physical linkage between WWBs and local deep convection, we here first examine their spatial co-location over eight regions (i.e., split into a northwestern, northern, northeastern, western, central, eastern, southern, and southeastern region of tropical Pacific) based on the study of Harrison and Vecchi (1997). Deep convection is defined when the OLR is less than 170 W/m<sup>2</sup>, following previous studies (Arkin and Meisner 1987; Evans and Shemo 1996; Hartten 1996). Figure 4 shows the composite deep convection anomalies over each region during days when WWBs occur at any grid point. It is evident that WWBs are closely related to local deep convection anomalies in all eight regions of the tropical Pacific. This spatial consistence between WWBs and local deep convections can also be observed in the high-frequency time scale (not shown).

Since WWBs are closely related to deep convection anomalies, we next explore the spatial and temporal features of deep convection during the El Niño evolution. Figure 5 shows the seasonal evolution of anomalous days of the deep convection over the tropical Pacific to characterize the deep convection activity during El Niño. During boreal autumn, climatological deep convection is mainly located in the Northern Hemisphere over the tropical Pacific, with the maximum being in the WNP and elongating zonally from the western Pacific to the western coast of Central America. Similarly, the El Niño-associated deep convection occurs more frequently relative to the climatology over the WNP and a zonal belt near 8°N of the central and eastern Pacific (Fig. 5a). In the following months, the anomalies of deep convection days show a pronounced southward shift with the center moving from 8°N to 6°S (Fig. 5c) along with the seasonal southward shift of climatological deep convection (not shown). During decaying spring (FMA(1)) when the South Pacific Convergence Zone (SPCZ) is the strongest (Vincent 1994), there are more frequent occurrences of deep convection south of the equator over the central Pacific (Fig. 5b). This meridional movement of deep convection anomalies could mediate the seasonal-varying features of WWBs along with the El Niño evolution.

As shown in Fig. 3, the El Niño SST anomalies during both ASO(0) and FMA(1) are quasi-symmetric with respect



Fig. 5 Composite spatial pattern of anomalous days of the deep convection (days per month) during the **a** developing autumn and **b** decaying spring of El Niño. **c** The composite monthly evolution of deep convection days averaged over the tropical Pacific (120°E-120°W) from July(0) to June(1) of El Niño. The deep convection is defined when the OLR is less than 170 W/m². Hatching indicates composite values that exceed the 90% significance level



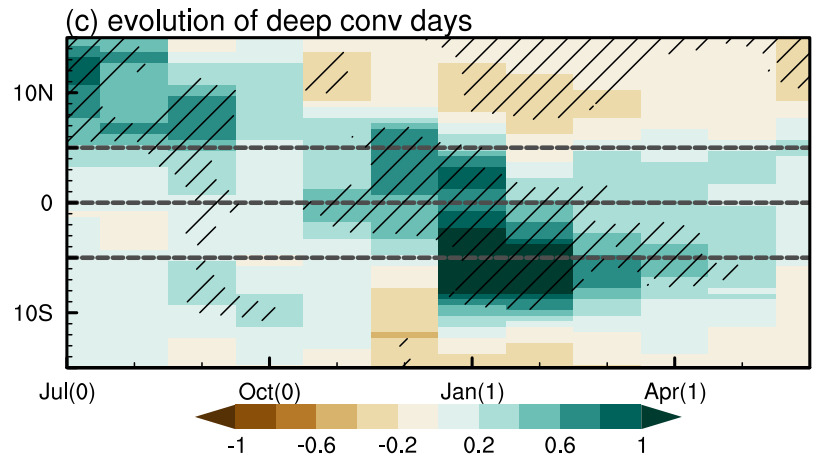
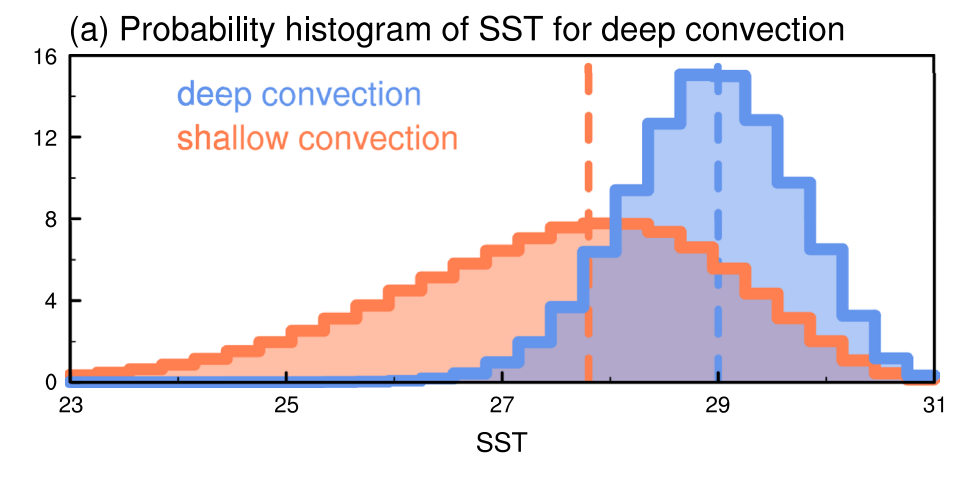
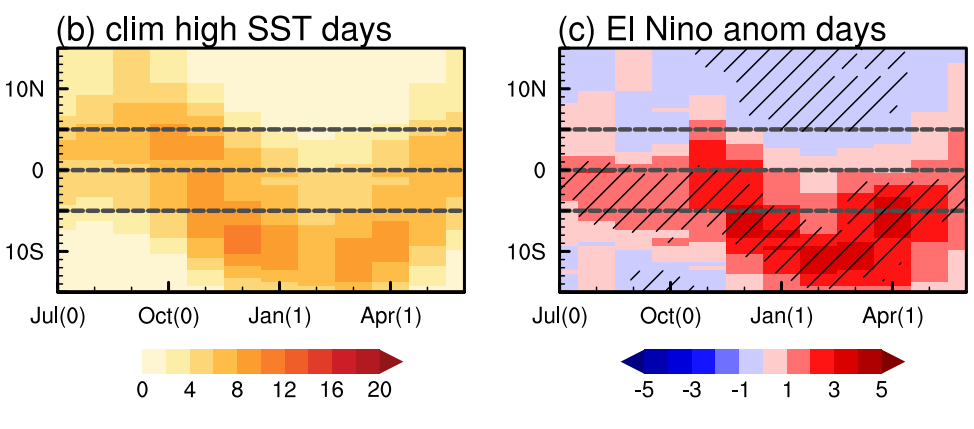


Fig. 6 a The probability histogram (%) of SST associated with deep (orange) and shallow (blue) convection in the region of 5°S-5°N, 170°E-120°W. Here, the SSTs are binned to every 0.5 °C, and then the corresponding probabilities are calculated. **b** The monthly evolution of climatological days with SSTs higher than 29 °C from autumn to next spring over the tropical Pacific ( $\overline{120}^{\circ}\text{E-}120^{\circ}\text{W}$ ). c The composite monthly evolution of anomalous days with high SSTs averaged over the tropical Pacific from July(0) to June(1) of El Niño. Hatching indicates composite values that exceed the 90% significance level







to the equator over the central and eastern Pacific. How do these equatorially quasi-symmetric SST anomalies lead to the asymmetric deep convection anomalies? In general, deep convection is accompanied by high SSTs (Zhang 1993; Lau et al. 1997; Sabin et al. 2013). As shown in Fig. 6a, the probability histogram of the underlying SSTs for deep convections exhibits its peak near 29.0 °C, different from that of shallow convection (OLR  $\geq 170 \text{W/m}^2$ ) with its peak near 27.8 °C. Notably, the distinction in the magnitude of SSTs for deep and shallow convection is also evident when comparing the upper percentile of the probability histogram (not shown). Previous studies have shown that the convection anomalies are closely linked to the underlying SSTs, including both the climatological SSTs and the superimposed SST anomalies (e.g., Gadgil et al. 1984; Graham and Barnett 1987), and therefore the seasonal movement of the climatological high SSTs could play an important role in the southward shift of deep convection anomalies. To characterize the meridional movement of climatological high SSTs, we summed the days of SSTs exceeding 29.0 °C at each latitude over the region of 120°E-120°W, where WWBs occur frequently, during each calendar month. Here the SST threshold of 29.0 °C is used to characterize deep convection.

We emphasize that our main conclusions remain almost the same for slight changes of the SST threshold from 28.5 °C to 29.5 °C (not shown). Figure 6b shows the southward movement of climatological high SST days from autumn to next spring along with the seasonal march of solar insolation. In autumn, the high SSTs are mainly located near and north of the equator (Fig. 6b). It can also be clearly seen from the spatial pattern that the climatological high SSTs tend to occur in the western warm pool region with a preference for staying near the equator and the northern hemisphere (Fig. 7a). In contrast, SSTs above 29.0 °C during spring are more likely to occur south of the equator (Fig. 6b), with the eastern boundary extending eastward towards 140°W (Fig. 7b). During the El Niño events, the overall seasonal evolution of anomalous days of high SSTs over the tropical Pacific exhibits similar features as that of climatological high SSTs, especially in terms of the southward movement (Fig. 6c). The El Niño-associated quasi-symmetric positive SST anomalies during the developing autumn lead to increased occurrences of high SSTs near and north of the equator over the central Pacific (Fig. 7c), therefore leading to more anomalous deep convection (Fig. 5a) and thus more frequent WWBs there (Fig. 3a, d). Correspondingly,

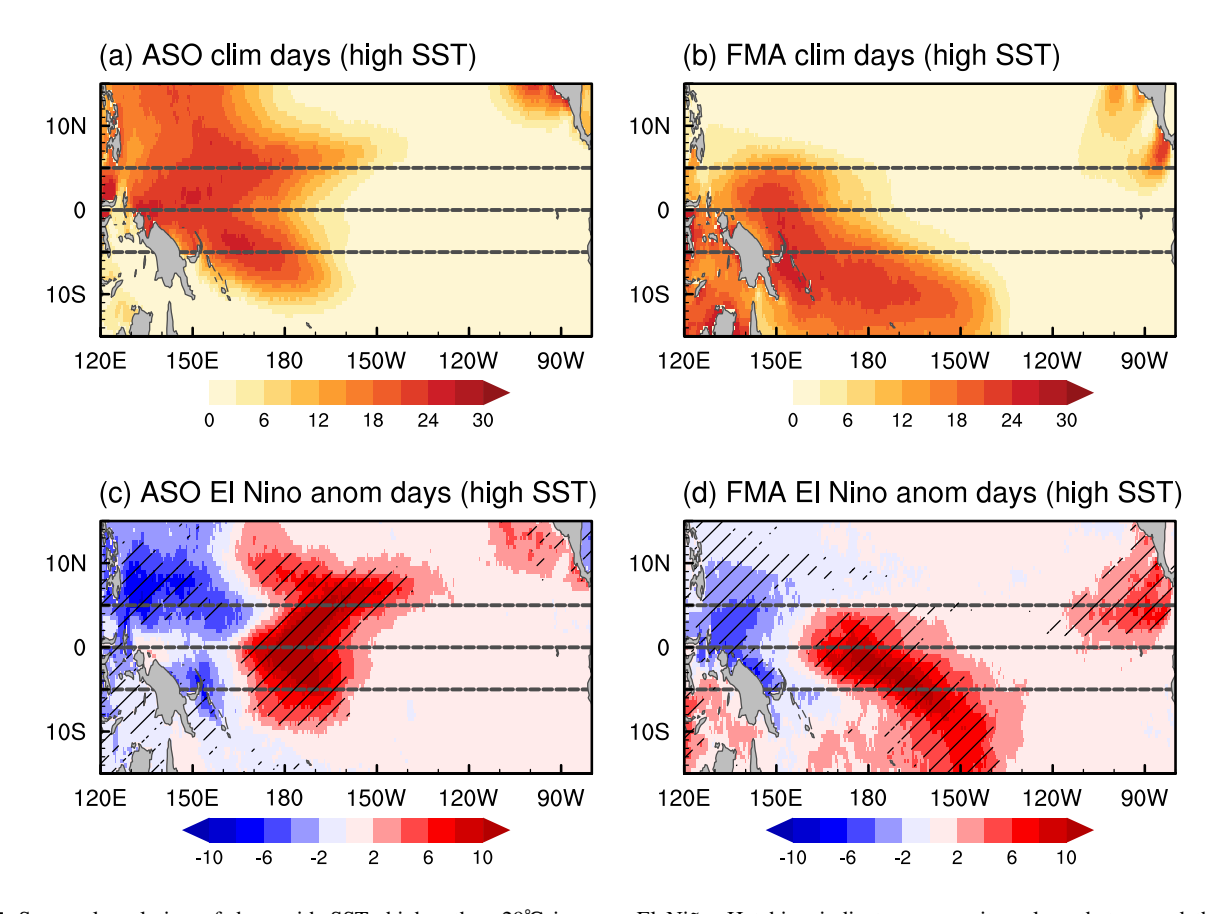


Fig. 7 Seasonal evolution of days with SSTs higher than  $29^{\circ}$ C in a autumn and b spring. The seasonal evolution of anomalous days with high SSTs during the c developing autumn and d decaying spring of

El Niño. Hatching indicates composite values that exceed the 90% significance level



during El Niño decaying spring, anomalous deep convection (Fig. 5b) and associated WWBs (Fig. 3b, e) are prone to occur in the Southern Hemisphere due to the southward displacement of high SSTs (Fig. 7d). It's notable that the anomalous days of high SSTs are larger than those of deep convections during El Niño events, indicating that high SSTs provide a necessary but not sufficient precondition for the occurrence of deep convections. In addition to high SSTs, several other factors could influence the development of deep convection, such as wind shear, atmospheric conditions aloft including upper-level divergence, jet streams (Grabowski and Clark 1993; Warren et al. 2017; Peter et al. 2022). The above analyses demonstrate the role of background annual cycle, particularly that of high SSTs and corresponding deep convection over the western-central Pacific, in modulating the seasonal-varying features of WWBs during El Niño events. It is noted that the equatorial WWBs exhibit zonal migration along with the El Niño evolution (Fig. 2), which could also be related to the nonlinear interaction process between El Niño and background annual cycle.

### 5 Resemblances of seasonal-varying features of WWBs in two flavors of El Niño

Previous studies have shown that the southward shift of zonal wind anomalies is more prominent during EP El Niño events than that during CP El Niño events, corresponding to the contrasting interaction processes between the western Pacific SST annual cycle and the two different flavors of El Niño (Zhang et al. 2015; Jiang et al. 2020). Here, in Fig. 8 we composite the monthly evolution of SST anomalies and WWBs at the equator during EP and CP El Niño separately to investigate whether the spatiotemporal characteristics of the high frequency part of zonal wind anomalies exhibit differences between the two flavors. In the equatorial region, large discrepancies in the seasonalvarying features of WWBs can be observed for the two El Niño flavors (Fig. 8). The WWB activity, identified by both M1 and M2, is generally enhanced and located further eastward during the whole lifecycle of EP El Niño events compared to CP El Niño events. This difference is closely related to the contrasting SST anomaly patterns of these two types of El Niño. Usually, EP El Niño has positive SST anomalies centered around 120°W with the maximum intensity being more than 3.0 °C (Fig. 8a), while CP El Niño has much weaker SST anomalies with their center shifted

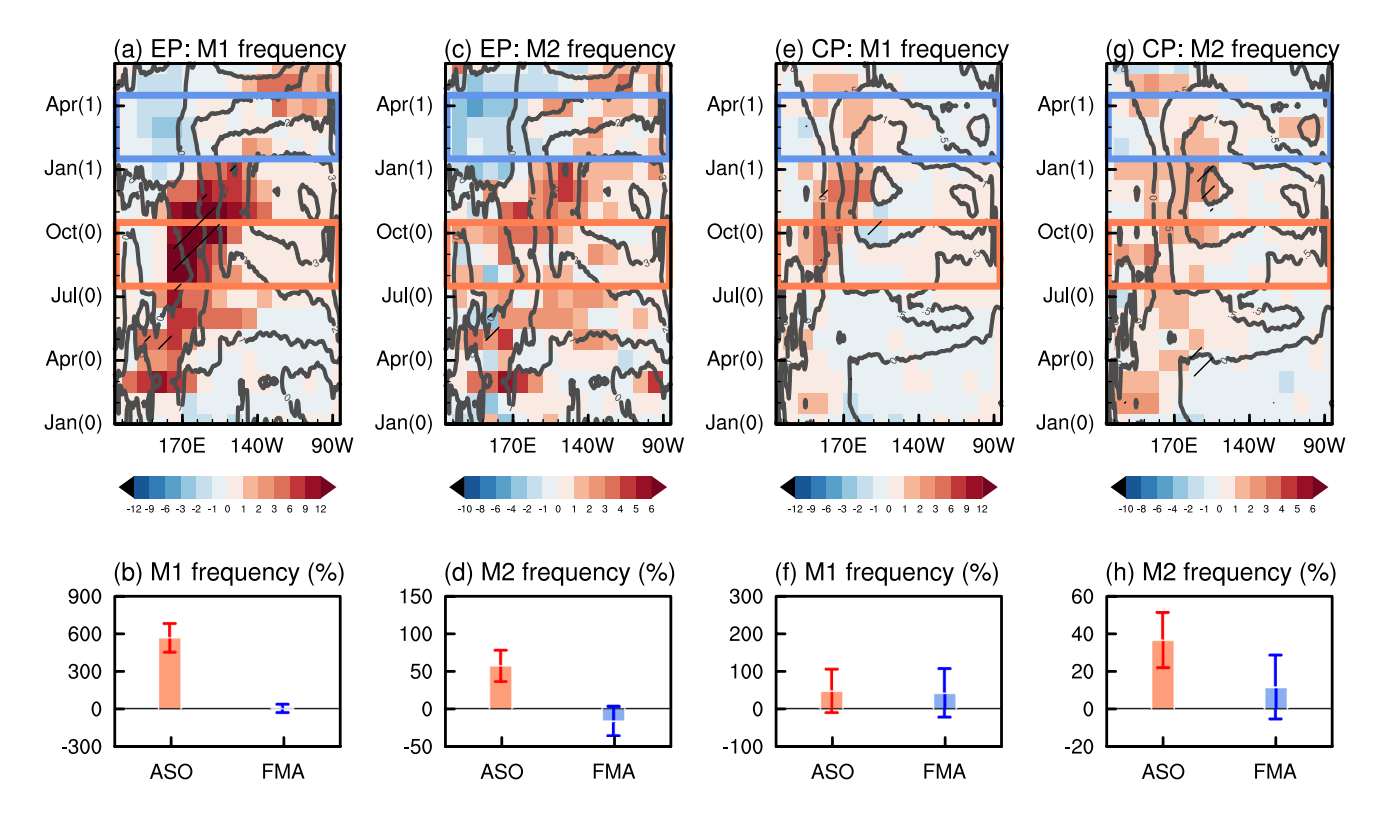


Fig. 8 As in Fig. 2a-b, e-f, but separated into a-d EP and e-h CP El Niño events. Here the contours for the EP and CP El Niño events are shown at intervals of 1.0 °C and 0.5 °C, respectively. Hatching indicates composite values that exceed the 90% significance level



westward to around 160°W (Fig. 8e). The SST anomaly pattern associated with EP El Niño tends to provide a more favorable condition for the occurrence of the deep convection and WWBs, leading to larger zonal expansion of WWBs, compared to CP El Niño. Besides, the seasonal evolution of the equatorial WWB activity also shows a large disparity for the two El Niño flavors despite that both types exhibit comparable amplitude of SST anomalies in ASO(0) and FMA(1). For the EP El Niño composite (Fig. 8a–d), the equatorial WWB activity is stronger in ASO(0) than in FMA(1), analogous to the composite of all El Niño events (Fig. 2). In contrast, for the CP El Niño composite (Fig. 8e–h), the WWB activity is quite similar between ASO(0) and FMA(1).

Nevertheless, the seasonal meridional migration of WWBs during the two El Niño flavors bear a close resemblance over the tropical Pacific. The composite spatial distributions of WWBs during EP and CP El Niño developing and decaying phases are shown in Figs. 9 and 10, respectively. For both EP and CP El Niño events, there appears remarkable southward displacement of WWBs along with the seasonal march of solar insolation. During the EP El Niño developing phase, WWBs are more frequently

detected near and north of the equator over the western Pacific, covering a large meridional extent from 15°N to 5°S (Fig. 9a, c). When the EP El Niño enters its decaying phase, the associated WWB activity is displaced southward and more frequent WWBs occur south of the equator (Fig. 9b, d). Focusing on a narrow equatorial band (e.g., 0.5°S-0.5°N or 2°S-2°N), the segmentary manifestation of the meridional migration could be mistaken for the evidence of a seasonal decrease of WWB activity during El Niño. During CP El Niño, the southward shift of WWBs is also prominent (Fig. 10b, d), though its extent is slightly weaker compared to that of EP El Niño (Fig. 9b, d). In the decaying spring of CP El Niño, pronounced WWB activity can be observed near and south of the equator (Fig. 10b, d). If we only focus on the equator, similar equatorial WWB activity is seen during both the developing and decaying phases. To sum up, the WWB activities during the two El Niño flavors exhibit similar spatiotemporal features regarding the seasonal meridional location. The similar southward-shifted characteristics of WWBs can be understood considering that the El Niño-associated deep convection anomalies are displaced southward for both El Niño flavors (Fig. 11).

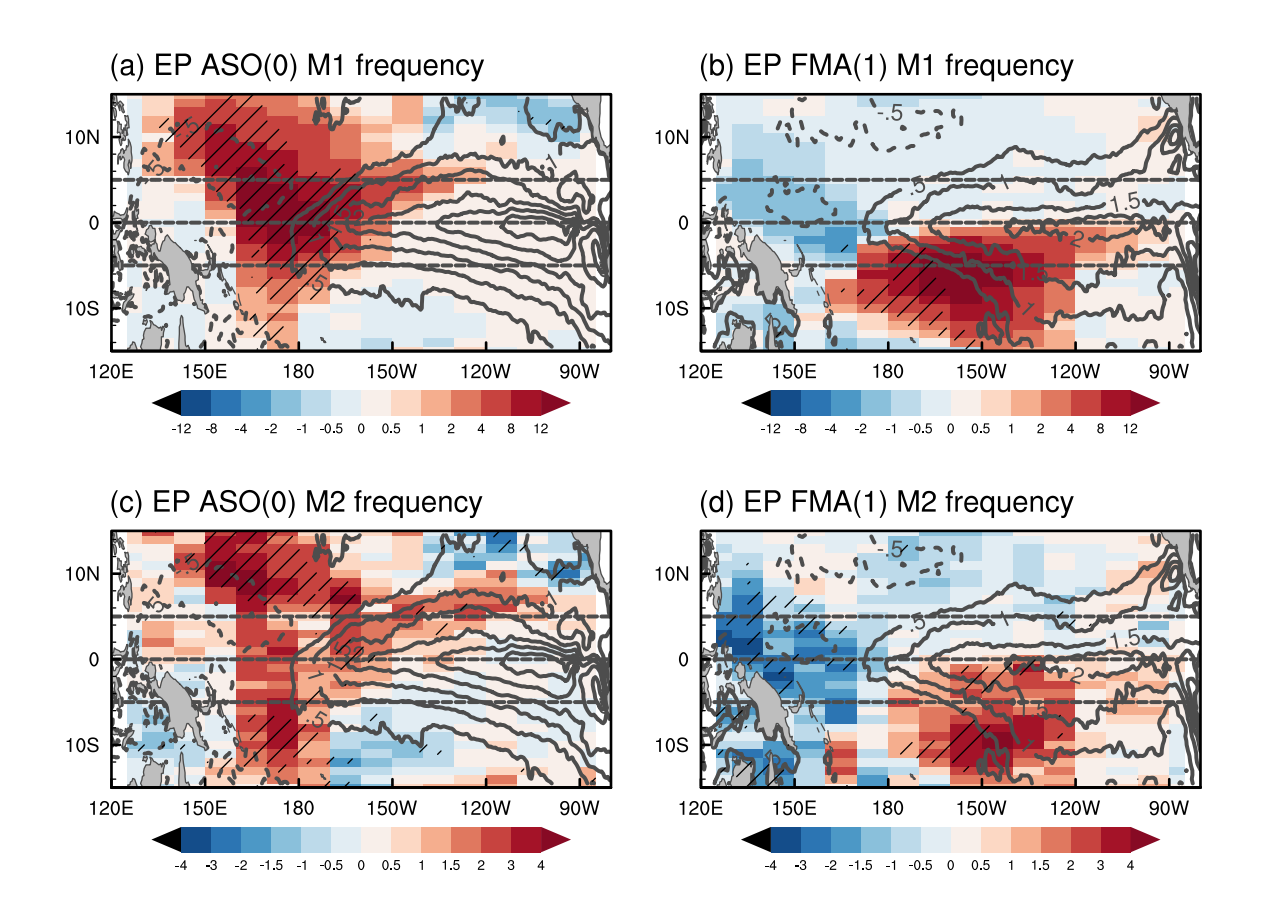


**Fig. 9** Composite spatial distribution of the SST anomaly ( $^{\circ}$ C; contours at intervals of 0.5  $^{\circ}$ C with zero contours omitted) and WWB frequency anomaly defined in M1 (days per month; shading) during **a** 

ASO(0) and **b** FMA(1) of the EP El Niño events  $\mathbf{c}$ -**d**. As in  $\mathbf{a}$ -**b**, but for the WWB frequency anomaly defined in M2. Hatching indicates composite values that exceed the 90% significance level



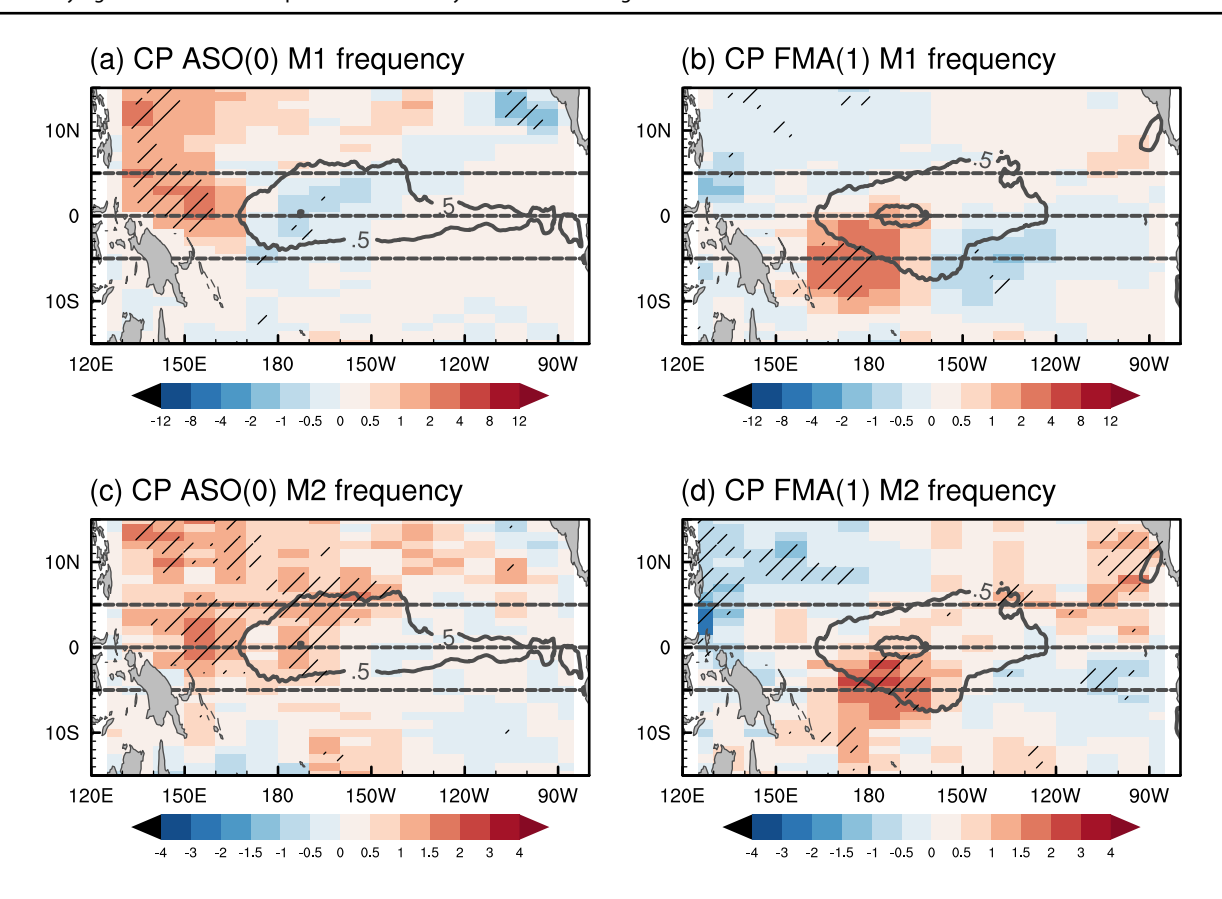


Fig. 10 As in Fig. 9, but for anomalies during the CP El Niño events. Here the contours are shown at intervals of  $0.5\,^{\circ}\mathrm{C}$ 

### 6 Conclusion and discussion

The relationship between ENSO and high-frequency atmospheric variability has been extensively studied in recent decades, reaching no clear consensus regarding cause and effect (e.g., McPhaden 1999; Lengaigne et al. 2004; Eisenman et al. 2005; Gebbie et al. 2007; Levine et al. 2017; Hayashi and Watanabe 2017; Lian and Chen 2021). While it is well-recognized that WWBs act to play an essential role in energizing ENSO, especially during the onset of an El Niño, multiple lines of evidence have indicated that WWBs can in turn be modulated by El Niño-related air-sea conditions throughout its whole lifecycle (e.g., Eisenman et al. 2005; Gebbie et al. 2007; Tziperman and Yu 2007; Seiki and Takayabu 2007). So far, the spatiotemporal features of WWBs during El Niño events have not been fully understood, and the underlying mechanism responsible for the seasonal variation along with the El Niño evolution remains unclear. In the present study, we find that the anomalous activity of WWBs—in terms of both frequency and accumulated strength—shifts noticeably southward from the developing boreal autumn to decaying spring of an El Niño event, regardless of the definition of WWBs used. This seasonally-varying feature is closely linked to the southward displacement of the El Niño-related deep convection. In El Niño developing autumn, the climatological high SSTs over the western-central Pacific are located mainly in the northern hemisphere, and the equatorially quasi-symmetric El Niñorelated SST anomalies can thus lead to more frequent SSTs above 29 °C near and north of the equator and increase the probability of the occurrence of deep convection and WWBs. During El Niño decaying spring, the climatological warm SSTs are shifted southward of the equator, allowing total SSTs to surpass the threshold for the deep convection in the Southern Hemisphere. Consequently, WWBs occur more frequently south of the equator during the decaying spring of El Niño. The so-called seasonal difference of equatorial WWB activity during El Niño is actually a segmentary manifestation of the strong meridional migration of WWB activity from the Northern to Southern Hemisphere following the seasonal march of the warm pool. This is an example of high-frequency transients, i.e., WWBs, being closely linked to the Combination Mode between ENSO and the warm pool annual cycle (Stuecker et al. 2013, 2015).

Furthermore, we find that there appears a close resemblance between the seasonal-varying features of WWB activity during EP and CP El Niño events in terms of the meridional migration, due to similar meridional shifts of deep convection anomalies. We emphasize that the seasonal-varying behavior of WWBs during two types of El Niño



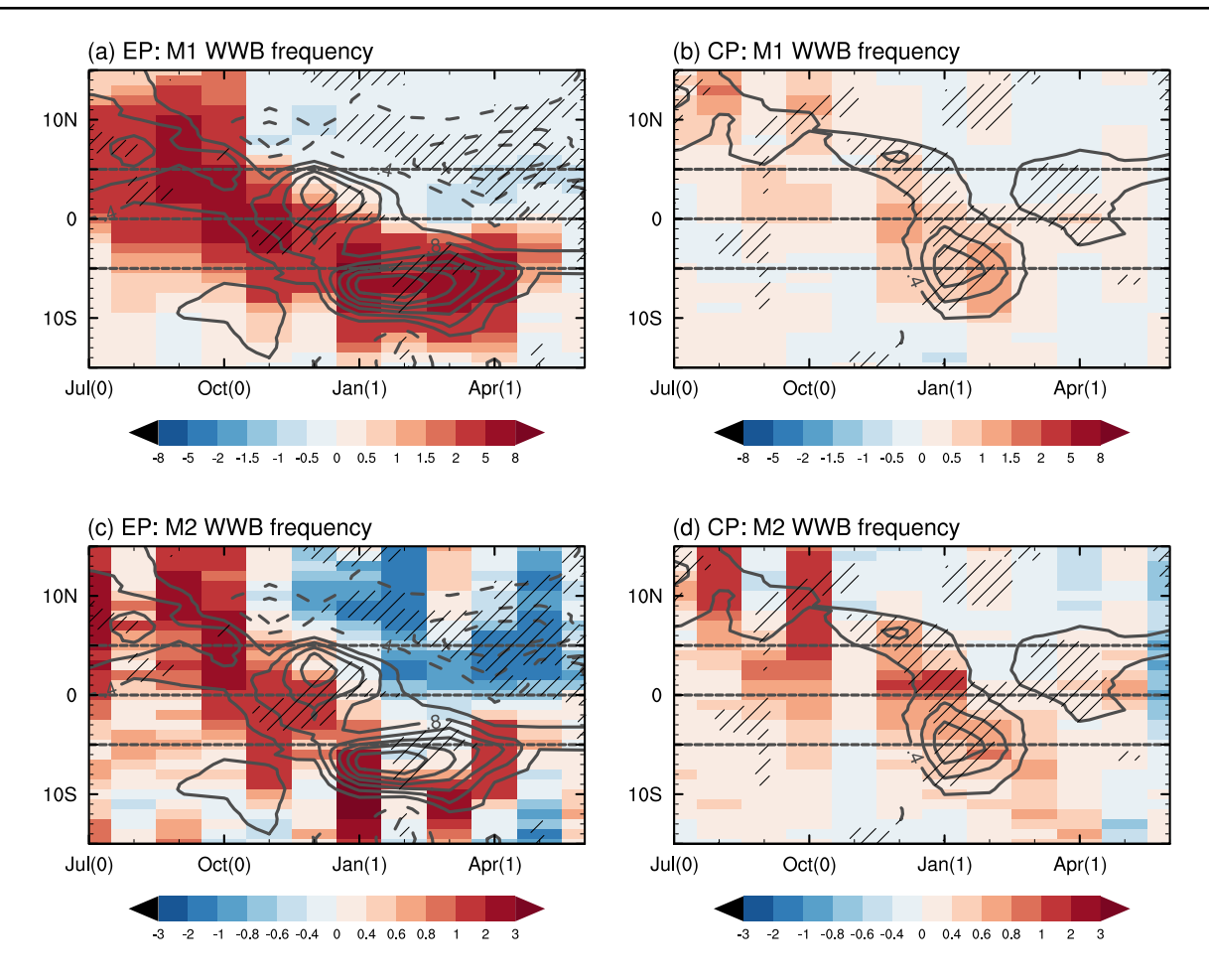


Fig. 11 Latitude-time section of the frequency anomaly of WWBs defined by M1 (days per month; shading) and anomalous deep convection days (contours) averaged between 120°E and 120°W for the

**a** EP El Niño and **b** CP El Niño events. **c**–**d** As in **a**–**b**, but for the WWB defined by M2. Hatching indicates composite anomalous deep convection days that exceed the 90% significance level

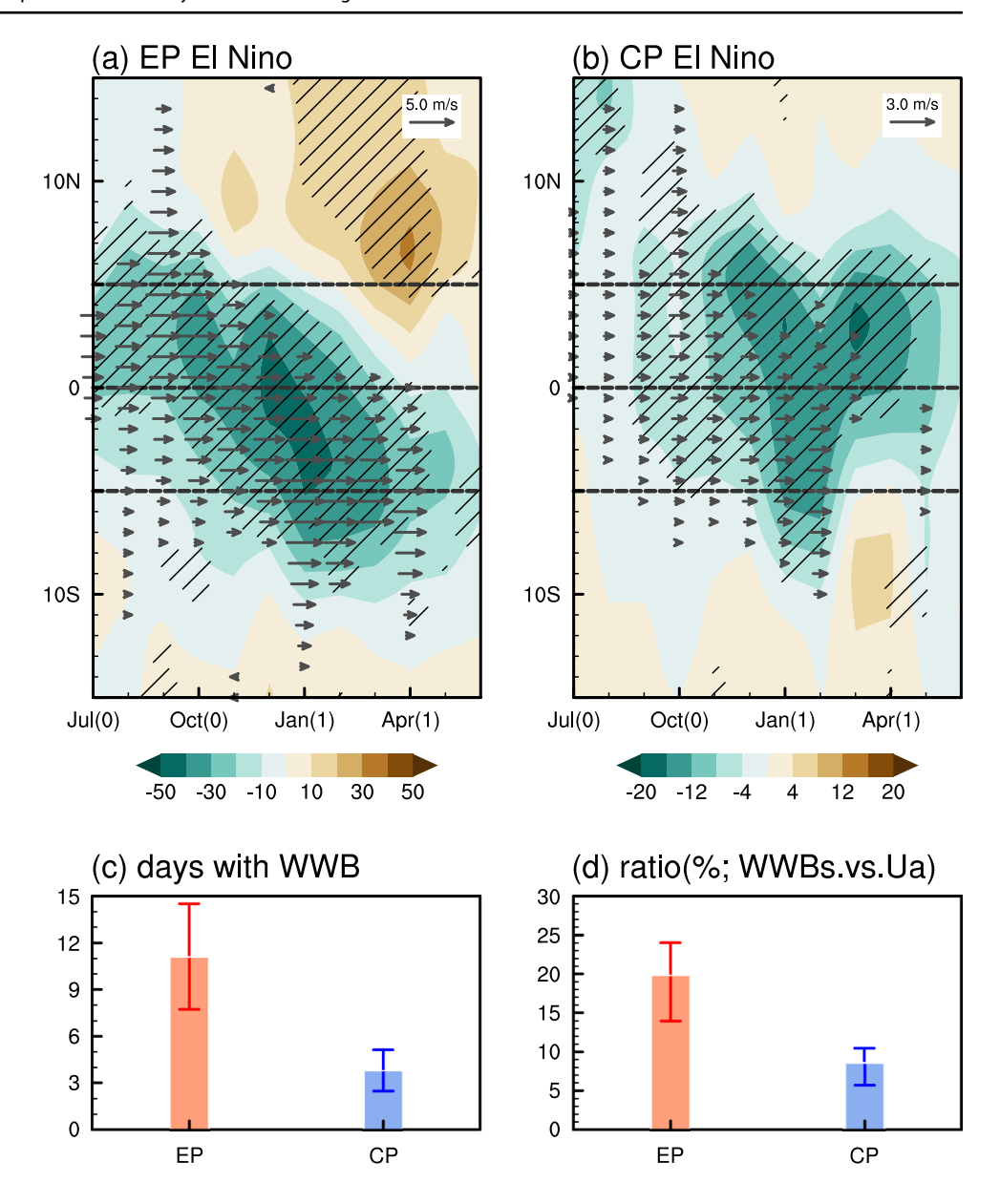
is to some extent different from those of monthly zonal wind anomalies as shown in many previous studies (e.g., McGregor et al. 2012, 2013; Zhang et al. 2015) (see also Fig. 12). The zonal wind and convection anomalies display a robust southward shift from the developing autumn to decaying spring of EP El Niño (Fig. 12a), while a weak meridional migration of the atmospheric anomalies is observed during CP El Niño (Fig. 12b). To understand this seemingly contradictory behavior of the seasonal-varying features of monthly atmospheric anomalies and the high-frequency counterpart (i.e., WWBs), the days with WWBs and the ratio of these to the days with positive zonal wind anomalies are calculated respectively over the region of 10°S-10°N and 150°E-120°W, where the southward shift of the westerly wind anomaly is prominent during FMA(1) (Fig. 12c). The FMA(1) season is chosen considering the large difference between the meridional structure of WWBs and monthly zonal wind anomalies during decaying spring. The proportion of WWB occurrences (Fig. 12d) during EP El Niño is twice as large as during CP El Niño, that is, WWBs during

EP El Niño constitute a larger portion of the total wind anomalies compared to during CP El Niño. The qualitative conclusion remains the same if narrowing down the computed region to the southern hemisphere (10°S-0°, not shown). This could be responsible for the inconsistency of the monthly wind anomalies and the high-frequency counterpart during CP El Niño.

In this study, we present a more comprehensive picture of the spatiotemporal characteristics of WWBs during El Niño events and the association with the two different flavors of El Niño. We here emphasize the modulation of ENSO on WWB activity during its developing autumn to decaying spring seasons. This study is thus complementary to many previous studies that emphasized the role of WWBs during the onset phase of El Niño during boreal spring. In this developing El Niño spring season the large-scale SST anomaly pattern has not been well established yet and WWBs are an important trigger (and/or amplifier) for the development of El Niño events (e.g., McPhaden 1999; Boulanger et al. 2001; Lengaigne et al. 2004;



Fig. 12 Latitude-time section of monthly zonal wind anomaly (m/s; vector) and OLR anomaly (W/m<sup>2</sup>; shading) averaged between 150°E and 120°W for the a EP El Niño and b CP El Niño events. Hatching indicates composite OLR anomalies that exceed the 90% significance level. c The averaged days with WWB over the tropical Pacific region (10°S-10°N, 150°E-120°W) during the EP and CP El Niño decaying spring (FMA (1)). The orange and blue error bars in c denote one standard deviation error estimates for EP and CP El Niño, respectively. **d** As in **c**, but for the ratio (%) of days with WWBs to days with positive zonal wind anomalies



Fedorov et al. 2015; Levine et al. 2016, 2017; Hayashi and Watanabe 2017). Our study suggests that more attention should be paid to the various ways in which WWBs interact with ENSO (including its diversity) and the warm pool annual cycle and to better understand the implications for ENSO seasonal predictability. Besides, deep convections are regarded as an important intermediary in the modulation of ENSO on WWB activity. Here we make no distinction between deep convections associated with the extratropical cold surges, tropical cyclones or the Madden-Julian Oscillation, which also exhibit a prominent seasonality during El Niño events (e.g., Chen et al. 2004; Gushchina and Dewitte 2012; Feng et al. 2015; Guo and Tan 2021). The relative contribution of these convection systems on the seasonal-varying features of WWBs need to be investigated in the near future.

**Acknowledgements** This work was supported by the National Nature Science Foundation of China (42088101). This is IPRC publication 1606, SOEST contribution 11700.

**Author contributions** All authors contributed to the study completion. Material preparation, data collection and analysis were performed by ZX. WZ and ZX mainly conceived and designed the analysis. WZ and FJ mainly reviewed and revised the manuscript. FFJ and MFS gave constructive suggestions and comments on the manuscript. All authors read and approved the final manuscript.

**Funding** WZ was supported by the National Nature Science Foundation of China (42088101). MFS was supported by NSF grant AGS-2141728 and NOAA's Climate Program Office's Modeling, Analysis, Predictions, and Projections (MAPP) program grant NA20OAR4310445.

**Data availability** All the datasets generated and/or analysed during the current study are available from the following resources: The OISST



data are openly available from NOAA PSL at https://psl.noaa.gov/data/gridded/data.noaa.oisst.v2.highres.html. The ERA5 data are also available online at https://www.ecmwf.int/en/forecasts/datasets/reanalysis-datasets/era5.

#### **Declarations**

**Conflict of interests** The authors have no relevant financial or non-financial interests to disclose.

#### References

- Arkin PA, Meisner BN (1987) The relationship between large-scale convective rainfall and cold cloud over the western hemisphere during 1982–84. Mon Weather Rev 115:51–74. https://doi.org/10.1175/1520-0493(1987)115%3c0051:TRBLSC%3e2.0.CO;2
- Ashok K, Behera SK, Rao SA et al (2007) El Niño Modoki and its possible teleconnection. J Geophys Res Oceans 112:C11007. https://doi.org/10.1029/2006JC003798
- Battisti DS, Sarachik ES (1995) Understanding and predicting ENSO. Rev Geophys 33:1367–1376. https://doi.org/10.1029/95RG00933
- Boulanger JP, Durand E, Duvel JP et al (2001) Role of non-linear oceanic processes in the response to westerly wind events: new implications for the 1997 El Niño onset. Geophys Res Lett 28:1603–1606. https://doi.org/10.1029/2000GL012364
- Capotondi A, Sardeshmukh PD, Ricciardulli L (2018) The nature of the stochastic wind forcing of ENSO. J Clim 31:8081–8099. https:// doi.org/10.1175/JCLI-D-17-0842.1
- Chen T, Huang W, Yooh J (2004) Interannual variation of the East Asian cold surge activity. J Clim 17:401–413. https://doi.org/10.1175/1520-0442(2004)0172.0.CO;2
- Chen D, Lian T, Fu C et al (2015) Strong influence of westerly wind bursts on El Niño diversity. Nat Geosci 8:339–345. https://doi.org/10.1038/ngeo2399
- Chiodi AM, Harrison DE, Vecchi GA (2014) Subseasonal atmospheric variability and El Niño waveguide warming: observed effects of the Madden–Julian oscillation and westerly wind events. J Clim 27:3619–3642. https://doi.org/10.1175/JCLI-D-13-00547.1
- Chu PS (1988) Extratropical forcing and the burst of equatorial westerlies in the western pacific: a synoptic study. J Meteorol Soc Jpn Ser II 66:549–564. https://doi.org/10.2151/jmsj1965.66.4\_549
- Eisenman I, Yu L, Tziperman E (2005) Westerly wind bursts: ENSO's tail rather than the dog? J Clim 18:5224–5238. https://doi.org/10.1175/JCL13588.1
- Evans JL, Shemo RE (1996) A procedure for automated satellite-based identification and climatology development of various classes of organized convection. J Appl Meteorol Climatol 35:638–652. https://doi.org/10.1175/1520-0450(1996)035%3c0638:APFASB% 3e2.0.CO;2
- Fasullo J, Webster PJ (2000) Atmospheric and surface variations during westerly wind bursts in the tropical western pacific. Q J R Meteorol Soc 126:899–924. https://doi.org/10.1002/qj.49712656407
- Fedorov AV, Hu S, Lengaigne M, Guilyardi E (2015) The impact of westerly wind bursts and ocean initial state on the development, and diversity of El Niño events. Clim Dyn 44:1381–1401. https://doi.org/10.1007/s00382-014-2126-4
- Feng J, Liu P, Chen W, Wang X (2015) Contrasting madden–julian oscillation activity during various stages of EP and CP El Niños. Atmos Sci Lett 16:32–37. https://doi.org/10.1002/asl2.516

- Fu M, Tziperman E (2019) Essential ingredients to the dynamics of westerly wind bursts. J Clim 32:5549–5565. https://doi.org/10.1175/JCLI-D-18-0584.1
- Fu M, Tziperman E (2021) A model study of the role of convection in westerly wind burst dynamics. J Clim 34:6235–6246. https://doi.org/10.1175/JCLI-D-20-0723.1
- Fu C, Diaz HF, Fletcher JO (1986) Characteristics of the response of sea surface temperature in the central Pacific associated with warm episodes of the Southern Oscillation. Mon Wea Rev 114:1716–1738. https://doi.org/10.1175/1520-0493(1986)1142.0.
- Gadgil S, Joseph PV, Joshi NV (1984) Ocean–atmosphere coupling over monsoon regions. Nature 312:141–143. https://doi.org/10.1038/312141a0
- Gebbie G, Eisenman I, Wittenberg A, Tziperman E (2007) Modulation of westerly wind bursts by sea surface temperature: a semistochastic feedback for ENSO. J Atmos Sci 64:3281–3295. https://doi.org/10.1175/JAS4029.1
- Gong Y, Li T (2022) Comparison of southward shift mechanisms of equatorial westerly anomalies between EP and CP El Niño. Clim Dyn 60:785–796. https://doi.org/10.1007/s00382-022-06346-6
- Grabowski WW, Clark TL (1993) Cloud-environment interface instability. Part III: direct influence of environmental shear. J Atmos Sci 67:3821–3828. https://doi.org/10.1175/1520-0469(1993)050%3c3821:CEIIPI%3e2.0.CO;2
- Graham NE, Barnett TP (1987) Sea surface temperature, surface wind divergence, and convection over tropical oceans. Sci New Ser 238:657–659. https://doi.org/10.1126/science.238.4827.657
- Guo Y, Tan Z (2021) Influence of different ENSO types on tropical cyclone rapid intensification over the western North Pacific. J Geophys Res Atmospheres 126:e2020JD033059. https://doi.org/ 10.1029/2020JD033059
- Gushchina D, Dewitte B (2012) Intraseasonal tropical atmospheric variability associated with the two flavors of El Niño. Mon Wea Rev 140:3669–3681. https://doi.org/10.1175/MWR-D-11-00267.1
- Harrison DE (1987) Monthly mean island surface winds in the central tropical pacific and El Niño events. Mon Wea Rev 115:3133–3145. https://doi.org/10.1175/1520-0493(1987)115%3c3133: MMISWI%3e2.0.CO;2
- Harrison DE, Giese BS (1991) Episodes of surface westerly winds as observed from islands in the western tropical pacific. J Geophys Res Oceans 96:3221–3237. https://doi.org/10.1029/90JC01775
- Harrison DE, Larkin NK (1998) El Niño-Southern Oscillation sea surface temperature and wind anomalies, 1946–1993. Rev Geophys 36:353–399. https://doi.org/10.1029/98RG00715
- Harrison DE, Vecchi GA (1997) Westerly wind events in the tropical Pacific, 1986–95. J Clim 10:3131–3156. https://doi.org/10.1175/1520-0442(1997)010%3c3131:WWEITT%3e2.0.CO;2
- Hartten LM (1996) Synoptic settings of westerly wind bursts. J Geophys Res Atmospheres 101:16997–17019. https://doi.org/ 10.1029/96JD00030
- Hayashi M, Watanabe M (2017) ENSO complexity induced by state dependence of westerly wind events. J Clim 30:3401–3420. https://doi.org/10.1175/JCLI-D-16-0406.1
- Hayashi M, Watanabe M (2019) Importance of background seasonality over the eastern equatorial Pacific in a coupled atmosphere-ocean response to westerly wind events. Clim Dyn 52:7309–7327. https://doi.org/10.1007/s00382-016-3481-0
- Hersbach H, Bell B, Berrisford P et al (2020) The ERA5 global reanalysis. Q J R Meteorol Soc 146:1999–2049. https://doi.org/10.1002/qj.3803
- Jiang F, Zhang W, Stuecker MF, Jin F-F (2020) Decadal change of combination mode spatiotemporal characteristics due to an ENSO regime shift. J Clim 33:5239–5251. https://doi.org/10.1175/ JCLI-D-19-0822.1



- Kao H-Y, Yu J-Y (2009) Contrasting Eastern-Pacific and central-pacific types of ENSO. J Clim 22:615–632. https://doi.org/10.1175/2008J CLI2309.1
- Keen RA (1982) The role of cross-equatorial tropical cyclone pairs in the Southern Oscillation. Mon Weather Rev 110:1405–1416. https://doi.org/10.1175/1520-0493(1982)110%3c1405:TROCET% 3e2.0.CO:2
- Kleeman R, Moore AM (1997) A theory for the limitation of ENSO predictability due to stochastic atmospheric transients. J Atmos Sci 54:753–767. https://doi.org/10.1175/1520-0469(1997)054% 3c0753:ATFTLO%3e2.0.CO;2
- Kug J-S, Jin F-F, An S-I (2009) Two types of el Niño events: cold tongue El Niño and warm pool El Niño. J Clim 22:1499–1515. https://doi.org/10.1175/2008JCLI2624.1
- Larkin NK, Harrison DE (2005) Global seasonal temperature and precipitation anomalies during El Niño autumn and winter. Geophys Res Lett 32:L16705. https://doi.org/10.1029/2005G L022860
- Lau K-M, Wu H-T, Bony S (1997) The role of large-scale atmospheric circulation in the relationship between tropical convection and sea surface temperature. J Clim 10:381–392. https://doi.org/10.1175/ 1520-0442(1997)010%3c0381:TROLSA%3e2.0.CO;2
- Lengaigne M, Guilyardi E, Boulanger J-P et al (2004) Triggering of El Niño by westerly wind events in a coupled general circulation model. Clim Dyn 23:601–620. https://doi.org/10.1007/s00382-004-0457-2
- Levine AFZ, Jin F-F, McPhaden MJ (2016) Extreme noise-extreme El Niño: how state-dependent noise forcing creates El Niño-La Niña asymmetry. J Clim 29:5483–5499. https://doi.org/10.1175/JCLI-D-16-0091.1
- Levine AFZ, Jin F-F, Stuecker MF (2017) A simple approach to quantifying the noise–ENSO interaction. Part II: the role of coupling between the warm pool and equatorial zonal wind anomalies. Clim Dyn 48:19–37. https://doi.org/10.1007/s00382-016-3268-3
- Lian T, Chen D (2021) The essential role of early-spring westerly wind burst in generating the centennial extreme 1997/98 El Niño. J Clim 1:1–38. https://doi.org/10.1175/JCLI-D-21-0010.1
- Lian T, Chen D, Tang Y et al (2018) Linkage between westerly wind bursts and tropical cyclones. Geophys Res Lett 45:11431–11438. https://doi.org/10.1029/2018GL079745
- Liang Y, Fedorov AV, Haertel P (2021) Intensification of westerly wind bursts caused by the coupling of the Madden-Julian Oscillation to SST during El Niño onset and development. Geophys Res Lett 48:e2020GL089395. https://doi.org/10.1029/2020GL089395
- McGregor S, Timmermann A, Schneider N, Stuecker MF, England MH (2012) The effect of the South Pacific convergence zone on the termination of El Niño events and the meridional asymmetry of ENSO. J Clim 25:5566–5586. https://doi.org/10.1175/JCLI-D-11-00332.1
- McGregor S, Ramesh N, Spence P et al (2013) Meridional movement of wind anomalies during ENSO events and their role in event termination. Geophys Res Lett 40:749–754. https://doi.org/10. 1002/grl.50136
- McGregor S, Timmermann A, Jin F-F, Kessler WS (2016) Charging El Niño with off-equatorial westerly wind events. Clim Dyn 47:1111–1125. https://doi.org/10.1007/s00382-015-2891-8
- McPhaden MJ (1999) Genesis and evolution of the 1997–98 El Nino. Science 283:950–954. https://doi.org/10.1126/science.283.5404. 950
- Meehl GA, Kiladis GN, Weickmann KM et al (1996) Modulation of equatorial subseasonal convective episodes by tropicalextratropical interaction in the Indian and Pacific Ocean regions. J Geophys Res Atmospheres 101:15033–15049. https://doi.org/ 10.1029/96JD01014

- Nitta T (1989) Development of a twin cyclone and westerly bursts during the initial phase of the 1986–87 El Nino. J Meteorol Soc Jpn Ser II 67:677–681. https://doi.org/10.2151/jmsj1965.67.4\_677
- Peters JM, Morrison H, Nelson TC, Marquis JN, Mulholland JP, Nowotarski CJ (2022) The influence of shear on deep convection initiation. Part I Theory J Atmos Sci 79:1669–1690. https://doi. org/10.1175/JAS-D-21-0145.1
- Puy M, Vialard J, Lengaigne M, Guilyardi E (2016) Modulation of equatorial Pacific westerly/easterly wind events by the Madden– Julian oscillation and convectively-coupled Rossby waves. Clim Dyn 46:2155–2178. https://doi.org/10.1007/s00382-015-2695-x
- Rasmusson EM, Carpenter TH (1982) Variations in tropical Sea surface temperature and surface wind fields associated with the Southern Oscillation/El Niño. Mon Weather Rev 110:354–384. https://doi.org/10.1175/1520-0493(1982)110%3c0354:VITSST%3e2.0.CO;2
- Ren H-L, Jin F-F (2011) Niño indices for two types of ENSO. Geophys Res Lett 38:L04704. https://doi.org/10.1029/2010GL046031
- Reynolds RW, Smith TM, Liu C et al (2007) Daily high-resolutionblended analyses for sea surface temperature. J Clim 20:5473– 5496. https://doi.org/10.1175/2007JCLI1824.1
- Sabin TP, Babu CA, Joseph PV (2013) SST–convection relation over tropical oceans. Int J Climatol 33:1424–1435. https://doi.org/10. 1002/joc.3522
- Seiki A, Takayabu YN (2007) Westerly wind bursts and their relationship with intraseasonal variations and ENSO. Part I Statistics Mon Weather Rev 135:3325–3345. https://doi.org/10.1175/MWR3477.1
- Stein K, Schneider N, Timmermann A, Jin F-F (2010) Seasonal synchronization of ENSO events in a linear stochastic model. J Clim 23:5629–5643. https://doi.org/10.1175/2010JCLI3292.1
- Stein K, Timmermann A, Schneider N et al (2014) ENSO seasonal synchronization theory. J Clim 27:5285–5310. https://doi.org/10.1175/JCLI-D-13-00525.1
- Stuecker MF, Jin F-F, Timmermann A, McGregor S (2015) Combination mode dynamics of the anomalous Northwest Pacific anticyclone. J Clim 28:1093–1111. https://doi.org/10.1175/ JCLJ-D-14-00225.1
- Stuecker MF, Timmermann A, Jin F-F et al (2013) A combination mode of the annual cycle and the El Niño/Southern Oscillation. Nat Geosci 6:540–544. https://doi.org/10.1038/ngeo1826
- Sun M, Li T, Chen L (2020) El Niño phase-dependent high-frequency variability in Western equatorial Pacific. Clim Dyn 55:2165–2184. https://doi.org/10.1007/s00382-020-05376-2
- Tziperman E, Yu L (2007) Quantifying the dependence of westerly wind bursts on the large-scale tropical Pacific SST. J Clim 20:2760–2768. https://doi.org/10.1175/JCLI4138a.1
- Vincent DG (1994) The South Pacific convergence zone (SPCZ): a review. Mon Wea Rev 122:1949–1970. https://doi.org/10.1175/1520-0493(1994)122%3c1949:TSPCZA%3e2.0.CO;2
- Warren RA, Richter H, Ramsay HA, Siems ST, Manton MJ (2017) Impact of variations in upper-level shear on simulated supercells. Mon Wea Rev 145:2659–2681. https://doi.org/10.1175/ MWR-D-16-0412.1
- Yu S, Fedorov AV (2020) The role of westerly wind bursts during different seasons versus ocean heat recharge in the development of extreme El Niño in climate models. Geophys Res Lett 47:e2020GL088381. https://doi.org/10.1029/2020GL088381
- Zhang C (1993) Large-scale variability of atmospheric deep convection in relation to sea surface temperature in the tropics. J Clim 6:1898–1913. https://doi.org/10.1175/1520-0442(1993)006% 3c1898:LSVOAD%3e2.0.CO;2
- Zhang W, Li H, Jin F-F et al (2015) The annual-cycle modulation of meridional asymmetry in ENSO's atmospheric response and its dependence on ENSO zonal structure. J Clim 28:5795–5812. https://doi.org/10.1175/JCLI-D-14-00724.1



**Publisher's Note** Springer Nature remains neutral with regard to jurisdictional claims in published maps and institutional affiliations.

Springer Nature or its licensor (e.g. a society or other partner) holds exclusive rights to this article under a publishing agreement with the

author(s) or other rightsholder(s); author self-archiving of the accepted manuscript version of this article is solely governed by the terms of such publishing agreement and applicable law.

